Wave to Wire Power Maximisation from a Wave Energy Converter

Adrian C.M O Sullivan
MaRei SFI research centre,
University College Cork,Ireland
e-mail: adrian.osullivan@umail.ucc.ie

Gordon Lightbody
MaRei SFI research centre,
University College Cork,Ireland
e-mail: gordon.lightbody@ucc.ie

***Abstract*—In this paper a back-to-back voltage source converter controlled linear permanent magnet generator (LPMG) is utilised as the power take off (PTO) for a point absorber wave energy converter system (WEC). It is shown that reactive control which seems promising when an ideal PTO is assumed, is actually infeasible with a real PTO as the electrical losses of the LPMG are excessive when the wave frequency is lower than the natural frequency. A Zero Order Hold (ZOH) and First Order Hold (FOH) Model Predictive Control (MPC) which maximises the mechanical power is first utilised. The two MPC systems show that more electrical power is extracted for a lower horizon when the MPC is optimised for mechanical power. The electrical losses from the LPMG and voltage source converter (VSC) are then incorporated in the cost function of the MPC systems and demonstrates significant improvements in the electrical power extracted when compared to the electrical power extracted via mechanical power optimisation. PTO force and heave displacement constraints are then incorporated into the optimisation, to further demonstrate the limitations of performance when a realistic PTO is utilised. It is shown here that the electrical power can be maximised, whilst the PTO force and heave displacement are shown to be within limits. The power quality from the ZOH MPC is then compared to the power quality from the FOH MPC.**

***Index Terms*—Reactive control, MPC, LPMG, Power maximisation, Constraints, Power quality, ZOH, FOH**

I. Introduction

This paper focuses on the maximisation of electrical power extracted from a point absorber that operates in heave mode. This is a linear system and is suited for array formations. There has been some research directed towards the mechanical design of the WEC, but recently there has been much work focusing on the maximisation of power extracted by improving the control of the device.

Reactive control [1] which is a classical control technique, based on linear wave theory, was one of the first methods to be developed. With reactive control maximum average power can be extracted from the incoming excitation wave. However it is well known that there are some drawbacks with reactive control. i) The PTO forces needed to extract the maximum average power would be unrealistic to implement as the technology needed to execute these excessive PTO forces is unavailable. ii) The non-causal relationship between wave elevation and excitation force, means that a prediction of the excitation force is needed for reactive control to be established.

Excitation force prediction is an ongoing research problem which has attracted some research, others have tried sub-optimal control methods where prediction methods are not needed [2]. In [3] the excitation force waveform was assumed to be within a narrow bandwidth. The non-causal relationship within this narrow frequency bandwidth was then approximated as constant hence converting it into a causal problem.

Latching is another common type of sub-optimal control [4]. It is effectively a hybrid control technique where the WEC is locked into place when there is zero velocity and is then released at the optimal time. The theory is based on monochromatic waves, nonetheless there have been attempts in developing this method to deal with irregular waves [5].

Recently research has moved away from classical control methods and are now entering a new era of more advanced control such as optimal control [6] and especially MPC [7]. In [8] MPC was used and compared with a sub-optimal reactive method. The sub-optimal reactive control depends on a look up table for the non-causal value which is selected by the instantaneous wave frequency. The instantaneous wave frequency is estimated from an Extended Kalman Filter (EKF) [9], [10]. This EKF makes the assumption that the excitation force is an amplitude modulated wave with a slowly changing frequency over time. In [11] and [12] MPC algorithms were developed which maximised the average power of the WEC using a ZOH MPC and the unconventional FOH MPC which showed promising results. Work such as [13] then continued on from [11] by investigating convexity issues of the optimisation problem.

In this paper a MPC will be developed for average electrical power maximisation. Many have looked into hydraulic PTO systems [14], synchronous generators with classical control [15], [16] and LPMG design [17], [18], [19]. There have also been attempts in maximising electrical power with a LPMG by using optimal control with a infinite horizon [20] and with a receding horizon [21]. In work presented here, the electrical power and its power quality will be analysed, showing the importance of controlling the LPMG and machine side converter within the limits of the system while producing maximum average electrical power and satisfactory electrical power quality.

II. Modelling

A. Hydrodynamics

In this work a point absorber, which is cylindrical in shape is utilised. Where this point absorber has a $5m$ radius with a hemispherical bottom, a draft of $10m$ and a natural frequency of $0.94\ rad.s^{-1}$. Linear wave theory is assumed to be acceptable for modelling the hydrodynamics of the WEC. The hydrodynamic forces are in the vertical plane since the system is in the heave motion only. The forces included in the model are the stiffness force, the radiation force, the excitation force and the PTO force exerted on the body.

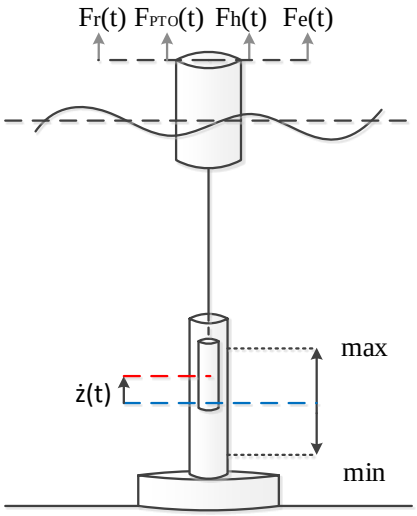

Fig. 1. System model with WEC and PTO

Together the forces form the hydrodynamic equation (1). The forces are shown here in the time domain where $\dot{z}(t)$ is the WEC velocity and M is the mass of the system.

$$M\ddot{z}(t) = F_h(t) + F_r(t) + F_e(t) + F_{PTO}(t) \tag{1}$$

The hydrodynamic model can then be extended by expressing the forces in terms of velocity and position as is shown in (2). Since the WEC is represented as a linear model the stiffness force $F_h(t)$ is represented as a product of the WEC displacement $z(t)$ and the hydrostatic stiffness β. Applying the Cummins transformation [22], the radiation force can then be represented as a convolution integral of the radiation kernel $h_r(t)$ and the velocity of the WEC. The radiation kernel and the added mass m_μ were found using WAMIT which is a boundary element method [23]. The PTO force is dependent on the type of control that is implemented on the system.

$$\ddot{z}(t) + \frac{1}{M+m_\mu}\int_{-\infty}^{t} h_r(t)\dot{z}(t-\tau)d\tau + \frac{\beta}{M+m_\mu}z(t) = u_c(t) + v_c(t) \tag{2}$$

$u_c(t)$ is a scaled version of $F_{PTO}(t)$ and $v_c(t)$ is scaled version of $F_e(t)$.

$$u_c(t) = \frac{F_{PTO}(t)}{M+m_\mu} \tag{3}$$

$$v_c(t) = \frac{F_e(t)}{M+m_\mu} \tag{4}$$

In the system the scaled excitation force $v_c(t)$ is an uncontrollable disturbance input unlike $u_c(t)$ which is a controllable input. The excitation force $F_e(t)$ is a function of the wave height $\eta(t)$, where the relationship is non-causal. The kernel $h_e(t)$ shown in (5) is found using WAMIT.

$$F_e(t) = \int_{-\infty}^{\infty} h_e(t)\eta(t+\tau)d\tau \tag{5}$$

Impulse response data for the radiation kernel function $h_r(t)$ is found using WAMIT. Using Prony's approximation the data is represented as a summation of exponential terms, as shown in (6). These exponential terms were then converted into a frequency domain transfer function. With this transfer function a singular value decomposition method is used to minimise the transfer function to the lowest possible order whilst maintaining the dominant characteristics of the full transfer function.

$$\begin{aligned} h_r(t) &= c_1e^{\mu_1 t} + c_2e^{\mu_2 t} + c_3e^{\mu_3 t} + c_4e^{\mu_4 t} + ... \\ \mathscr{L}\{h_r(t)\} = H_r(s) &= \frac{a_1s^{n_1} + a_2s^{n_2} + a_3s^{n_3}...}{s^{m_1} + b_1s^{m_2} + b_2s^{m_3}...} \end{aligned} \tag{6}$$

A state space model in the control canonical form was then developed to represent the transfer function in the time domain.

$$\begin{aligned} \dot{\boldsymbol{x_r}}(t) &= A_r\boldsymbol{x_r}(t) + B_r\dot{z}(t) \\ \boldsymbol{F_r}(t) &= C_r\boldsymbol{x_r}(t) + D_r\dot{z}(t) \end{aligned} \tag{7}$$

where $\boldsymbol{x_r}(t) \in \mathbb{R}^{n\times 1}$,$A_r \in \mathbb{R}^{n\times n}$,$B_r \in \mathbb{R}^{n\times 1}$, $C_r \in \mathbb{R}^{1\times n}$,$D_r \in \mathbb{R}^{1\times 1}$. The states of the system $\boldsymbol{x_c}(t)$ and the outputs $\boldsymbol{y_c}(t)$ of the continuous model are defined as the following

$$\boldsymbol{x_c}(t) = \begin{bmatrix} z(t) \\ \dot{z}(t) \\ \boldsymbol{x_r}(t) \end{bmatrix} \in \mathbb{R}^{(n+2)\times 1} \tag{8}$$

$$\boldsymbol{y_c}(t) = \begin{bmatrix} z(t) \\ \dot{z}(t) \end{bmatrix} \in \mathbb{R}^{2\times 1} \tag{9}$$

III. Model Predictive Control

With conventional MPC the systems cost function is minimised; this cost function is usually the sum of the squared error between the desired set point trajectory and the output of the system. For this system however, a reference trajectory is not available and the objective is to maximise the average power function as shown in (10).

$$P_{avg} = -\frac{1}{T}\int_{t=0}^{T} F_{PTO}(t)\dot{z}(t)dt \tag{10}$$

Ideally the discrete cost function used in the MPC would be an accurate approximation of the average power (10). The accuracy of this approximation will depend on the type of hold assumed for the PTO force. If a ZOH is assumed, then the PTO force is piecewise constant over the sample time, as shown in Fig. 2. A suitable approximation here is a Eulers/trapezoidal hybrid, which incorporates the piecewise constant PTO force and a piecewise linear approximation for the velocity over the sample time.

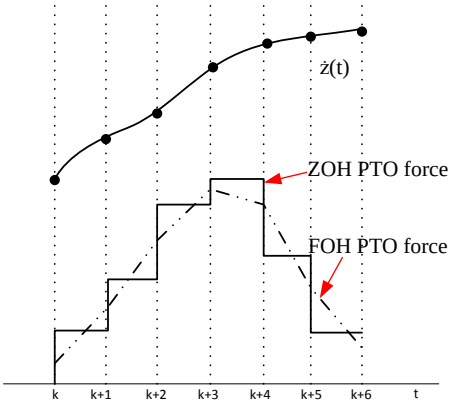

Fig. 2. Waveforms of (i) continuous WEC $\dot{z}(t)$ with sample points (ii)Piecewise constant PTO force from a ZOH controller (iii)Piecewise linear PTO force from a FOH controller

To increase the accuracy of the power extraction a FOH MPC was employed. The FOH allows the PTO force to be represented as a piecewise linear motion instead of a piecewise constant as shown in Fig.2. Since the FOH PTO force is piecewise linear it then allows a traditional trapezoidal rule to be implemented.

A. Zero Order Hold MPC

In order to maximise the average mechanical power extracted (10), the following discrete-time cost function, (11), needs to be minimised over the receding horizon N.

$$J_z(k) = \sum_{i=1}^{N} u_d(k+i-1)\left[\dot{z}(k+i) - \frac{\Delta\dot{z}(k+i)}{2}\right] \tag{11}$$

The system model was converted from the continuous to the discrete domain.

$$\begin{aligned} \boldsymbol{x}(k+1) &= A_d\boldsymbol{x}(k) + B_d u_d(k) + F_d v_d(k) \\ \boldsymbol{y_d}(k) &= C_d\boldsymbol{x}(k) \end{aligned} \tag{12}$$

$$A_d = e^{\boldsymbol{A_c}T_L} \in \mathbb{R}^{(n+2)\times(n+2)}$$

$$B_d = \int_{\eta=0}^{T_L} e^{\boldsymbol{A_c}\eta} B_c d\eta \in \mathbb{R}^{(n+2)\times 1}$$

$$F_d = \int_{\eta=0}^{T_L} e^{\boldsymbol{A_c}\eta} F_c d\eta \in \mathbb{R}^{(n+2)\times 1}$$

$$C_d = \begin{bmatrix} 1 & 0 & 0\cdots 0 \\ 0 & 1 & 0\cdots 0 \end{bmatrix} \in \mathbb{R}^{2\times(n+2)}$$

where A_c, B_c and C_c are the matrices of the continuous system and T_L is the outer mechanical sampling time. Integral action can then be incorporated by augmenting the model to form the augmented version as shown in equation (14).

$$\Delta u_z(k) = u_d(k) - u_d(k-1) \tag{13}$$

$$\begin{aligned} \boldsymbol{x_z}(k+1) &= A_z\boldsymbol{x_z}(k) + B_z\Delta u_z(k) + F_z\Delta v_z(k) \\ \boldsymbol{y_z}(k) &= C_z\boldsymbol{x_z}(k) \end{aligned} \tag{14}$$

$$A_z = \left[\begin{array}{c|ccc} A_d & \mathbf{0} & \mathbf{0} & \mathbf{0} \\ \hline \mathbf{0} & 1 & 0 & 0 \\ \mathbf{0} & 0 & 1 & 0 \\ \Upsilon\left(A_d - I\right) & 0 & 0 & 0 \end{array}\right] \in \mathbb{R}^{(n+5)\times(n+5)}$$

$$B_z = \left[\begin{array}{c} B_d \\ \hline 1 \\ 0 \\ \Upsilon B_d \end{array}\right] \quad F_z = \left[\begin{array}{c} F_d \\ \hline 0 \\ 1 \\ \Upsilon F_d \end{array}\right] \in \mathbb{R}^{(n+5)\times 1}$$

$$C_z = \left[\begin{array}{c|ccc} C_d & \mathbf{0} & \mathbf{0} & \mathbf{0} \\ \hline \mathbf{0} & 1 & 0 & 0 \\ \mathbf{0} & 0 & 0 & 1 \end{array}\right] \in \mathbb{R}^{4\times(n+5)}$$

$$\boldsymbol{x_z}(k) = \left[\begin{array}{c} \boldsymbol{x}(k) \\ \hline u_d(k-1) \\ v_d(k-1) \\ \Delta\dot{z}(k) \end{array}\right] \quad \boldsymbol{y_z}(k) = \left[\begin{array}{c} z(k) \\ \dot{z}(k) \\ \hline u_d(k-1) \\ \Delta\dot{z}(k) \end{array}\right]$$

where

$$\Upsilon = \begin{bmatrix} 0 & 1 & 0 & \cdots & 0 \end{bmatrix} \in \mathbb{R}^{1\times(n+5)}$$

B. First Order Hold MPC

Like the ZOH MPC the cost function representing the average power is maximised when the cost function is minimised over the prediction horizon N.

$$J_f(k) = \frac{1}{2}u_d(k+N)\dot{z}(k+N) + \sum_{i=1}^{N-1} u_d(k+i)\dot{z}(k+i) \tag{15}$$

The structure of the system with the FOH is similar to the ZOH method except that the inputs of the system are shifted into the future by one sample [12].

$$\begin{aligned} \boldsymbol{x_f}(k+1) &= A_f\boldsymbol{x_f}(k) + B_f\Delta u_f(k+1) + F_f\Delta v_f(k+1) \\ \boldsymbol{y_f}(k) &= C_f\boldsymbol{x_f}(k) \end{aligned} \tag{16}$$

$$\boldsymbol{x_f}(k) = \begin{bmatrix} \boldsymbol{x}(k) \\ u_d(k) \\ v_d(k) \end{bmatrix} \quad \boldsymbol{y_f}(k) = \begin{bmatrix} z(k) \\ \dot{z}(k) \\ u_d(k) \end{bmatrix}$$

$$A_f = \begin{bmatrix} e^{A_cT_L} & \Lambda & \Lambda \\ \mathbf{0} & 1 & 0 \\ \mathbf{0} & 0 & 1 \end{bmatrix} \in \mathbb{R}^{(n+4)\times(n+4)}$$

$$B_f = \begin{bmatrix} \Gamma \\ 0 \\ 1 \end{bmatrix} \quad B_f = \begin{bmatrix} \Gamma \\ 1 \\ 0 \end{bmatrix} \in \mathbb{R}^{(n+4)\times 1}$$

where $\Lambda = A_c^{-1}\left(e^{A_cT_L} - I\right)B_c \in \mathbb{R}^{(n+2)\times 1}$ and $\Gamma = \frac{1}{T_L}A_c^{-1}\left(\Lambda - T_LB_c\right) \in \mathbb{R}^{(n+2)\times 1}$

C. System Prediction

The outputs over a receding horizon from the system with a ZOH configuration were predicted, assuming the states are measured and the excitation wave force is known over the horizon.

$$\hat{\boldsymbol{y}}_{\boldsymbol{z}}(k) = P\boldsymbol{x}_{\boldsymbol{z}}(k) + Ha\boldsymbol{\Delta}\hat{\boldsymbol{u}}_{\boldsymbol{z}}(k) + Hw\boldsymbol{\Delta}\hat{\boldsymbol{v}}_{\boldsymbol{z}}(k) \tag{17}$$

where

$$P = \begin{bmatrix} CA \\ CA^2 \\ \vdots \\ CA^N \end{bmatrix} \hat{\boldsymbol{y}}_{\boldsymbol{z}}(k) = \begin{bmatrix} y_z(k+1) \\ \vdots \\ y_z(k+N) \end{bmatrix} \tag{18}$$

where $P \in \mathbb{R}^{4N\times(n+4)}$ and $\hat{\boldsymbol{y}}_{\boldsymbol{z}}(k), \hat{\boldsymbol{u}}_{\boldsymbol{z}}(k), \hat{\boldsymbol{v}}_{\boldsymbol{z}}(k) \in \mathbb{R}^{4N\times 1}$

$$Ha = \begin{bmatrix} CB & 0 & .. & 0 \\ CAB & CB & .. & 0 \\ \vdots & \vdots & \ddots & \vdots \\ CA^{N-1}B & CA^{N-2}B & .. & CB \end{bmatrix} \in \mathbb{R}^{4N\times N} \tag{19}$$

$$Hw = \begin{bmatrix} CF & 0 & .. & 0 \\ CAF & CF & .. & 0 \\ \vdots & \vdots & \ddots & \vdots \\ CA^{N-1}F & CA^{N-2}F & .. & CF \end{bmatrix} \in \mathbb{R}^{4N\times N} \tag{20}$$

By using the predicted outputs (17), the cost function in the summation form (15) can then be represented in matrix (21).

$$J_z(k) = \frac{1}{2}\hat{\boldsymbol{y}}_{\boldsymbol{z}}(k)^T Q_z \hat{\boldsymbol{y}}_{\boldsymbol{z}}(k) \tag{21}$$

where $Q_z \in \mathbb{R}^{4N\times 4N}$(22) and $Q_f \in \mathbb{R}^{3N\times 3N}$.

$$Q_z = \begin{bmatrix} M_z & 0 & .. & 0 \\ 0 & M_z & .. & 0 \\ \vdots & \vdots & \ddots & \vdots \\ 0 & 0 & 0 & M_z \end{bmatrix}$$
$$M_z = \begin{bmatrix} 0 & 0 & 0 & 0 \\ 0 & 0 & 1 & 0 \\ 0 & 1 & 0 & \frac{-1}{2} \\ 0 & 0 & \frac{-1}{2} & 0 \end{bmatrix} \tag{22}$$

The Hessian matrices of both ZOH and FOH costs have different dimensions to each other due to the size of the state matrices of both systems. The FOH cost function is similar to (21) except that the computation order is smaller than that of the ZOH system due to having one less state in its state matrix, where the FOH cost function formulation is shown in [12]. Quadratic programming (QP) methods available in packages such as MATLAB [24] or AMPL [25] can be used to minimise such cost functions within a receding horizon scheme and subject to constraints. The optimal $\Delta u_z(k)$ is obtained, and the process is repeated at the next sample, within the receding horizon scheme.

IV. Electrical power Optimisation

A. Linear Permanent Magnet Generator PTO

The PTO used was an LPMG [17] which was connected to a machine side back-to-back voltage source converter. The converter is made up of IGBT transistors that switch in a certain sequence allowing the average controller voltage to control the bidirectional power flow to the LPMG. The LPMG and machine side converter can then be represented in the dq domain [26] which are shown in (23) and (24). With the LPMG connected to the machine side converter the electrical characteristics and mechanical torque can be controlled (25).

$$L\frac{di_q}{dt} = -i_q(t)R - v_q(t) + \frac{\pi}{\tau}\dot{z}(t)\lambda_{fd}^{'} - \frac{\pi}{\tau}\dot{z}(t)Li_d(t) \tag{23}$$

$$L\frac{di_d}{dt} = -i_d(t)R - v_d(t) + \frac{\pi}{\tau}\dot{z}(t)Li_q(t) \tag{24}$$

$$F_{PTO}(t) = -\frac{p}{2}\lambda_{fd}i_q(t)\frac{\pi}{\tau} = -\lambda_{fd}^{'}i_q(t)\frac{\pi}{\tau} \tag{25}$$

where λ_{fd} is the flux linkage, p is the number of poles and τ is the pole pitch.

$$\frac{p}{2}\lambda_{fd} = \lambda_{fd}^{'} = \sqrt{\frac{3}{2}}46Wb \quad \text{and} \quad \tau = 0.1m$$

A major focus of wave energy research in recent years has been to maximise average power absorbed. There has been some interest in the realistic problems associated with non-ideal PTO systems, however classic control methods are still being used. For a cylindrical shaped WEC the maximum available average absorbed power is shown in Fig. 3. In the wave energy industry the classical control theory to maximise output average power is called reactive control; where the PTO force is controlled so that the maximum WEC velocity is in phase with the excitation force. Using an ideal PTO,

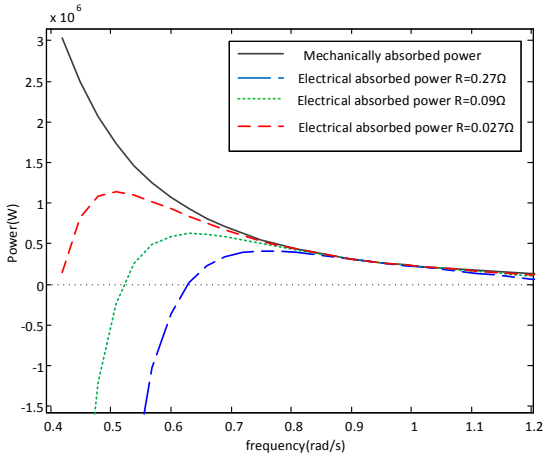

Fig. 3. Average power extracted from monochromatic waves using Reactive control with an (i)ideal PTO (Mechanically absorbed power) (ii)LPMG with realistic resistance of 0.27Ω (iii)LPMG with resistance of 0.09Ω (iv)LPMG with resistance of 0.027Ω

the average electrical power extracted from the system is the same as the average mechanical power. However when the non-idealities are included in the PTO the losses from the LPMG and converter become apparent, as can be seen in

Fig.3. The figure shows the electrical power diminishing at lower frequencies. This occurs due to the high instantaneous forces needed, requiring large currents and incurring large i^2R losses. The only way that the mechanically optimised average power cost would be sufficient for maximising the electrical power is if the flux linkage was unreasonably large and the resistance was unrealistically low. Hence it is essential that the electrical losses are included in the power maximisation.

B. Electrical Power MPC

The control scheme for the ZOH MPC is shown in Fig.4. The MPC requires measurements of the hydrodynamic system states and the predicted excitation force over the prediction horizon. To simplify the optimisation ,it is assumed in this initial study that there is no field weakening, and hence the d-axis current $i_d(t)$ is regulated as $0A$. This leaves a direct relationship between the PTO force and the $i_q(t)$ current. For the average electrical power to be maximised the cost function (10) must include the losses of the LPMG (26). The MPC then sends the optimal q-axis current setpoint to the faster inner current control loop of the cascade control which controls the force produced from the LPMG.

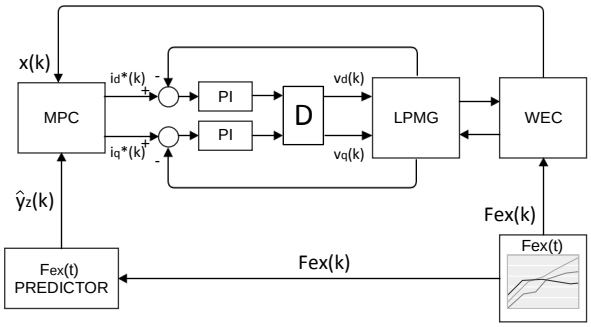

Fig. 4. Cascade formation of the faster loop controlling the LPMG dynamics and the slower outer loop controlling the mechanical dynamics of the system via MPC ($D = decoupler$)

$$P_{loss} = \frac{1}{T}\int_0^T i_q^2(t)Rdt \tag{26}$$

$$P_{loss}(k) = R\left(\frac{M+m_\mu}{\lambda'_{fd}\frac{\pi}{\tau}}\right)^2 \sum_{i=1}^{N} u_d^2(k+i-1) \tag{27}$$

From (3) and (25) the scaled PTO force can be related to the current of the LPMG (27). When the losses are included in the original ZOH cost function, the electrical cost of (28) results.

$$J(k) = \sum_{i=1}^{N} u_d(k+i-1)\left[\dot{z}(k+i) - \frac{\Delta\dot{z}(k+i)}{2}\right] + \frac{R(M+m_\mu)}{(\lambda'_{fd}\frac{\pi}{\tau})^2}\sum_{i=1}^{N} u_d^2(k+i-1) \tag{28}$$

The overall cost function can be developed with the same structure (22), but with M_z replaced by M_{zelec}.

$$M_{zelec} = \begin{bmatrix} 0 & 0 & 0 & 0 \\ 0 & 0 & 1 & 0 \\ 0 & 1 & 2G & -\frac{1}{2} \\ 0 & 0 & -\frac{1}{2} & 0 \end{bmatrix} \tag{29}$$

where

$$G = \frac{R(M+m_\mu)}{(\lambda'_{fd}\frac{\pi}{\tau})^2}$$

The format for the FOH electrical cost function can also be easily developed.

V. Simulation Results

A. Mechanical power maximisation

Initially the mechanical power cost function (11) was utilised. As the prediction horizon N increases the mechanical power absorbed approaches the ideal maximum, as shown in Fig. 5. However it is also shown in Fig.5 that for a shorter prediction horizon N the electrical extracted power is actually better than obtained with a longer horizon. As the mechanical power absorbed converges towards the ideal maximum, excessive PTO forces are required and hence the current $i_q(t)$ must be large (assuming that $i_d(t) = 0$), and electrical losses increase.

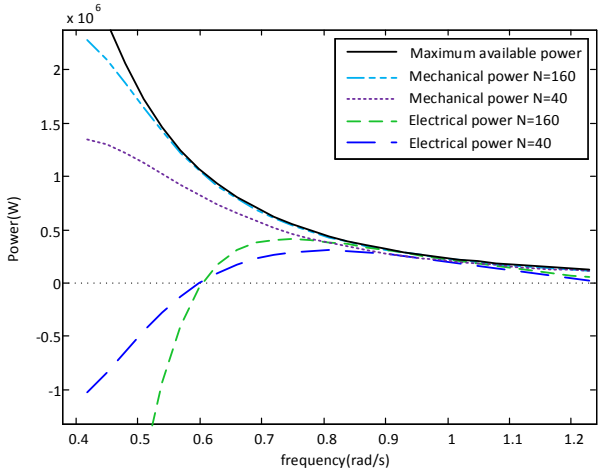

Fig. 5. Average power extracted from monochromatic waves via a LPMG with MPC optimised without LPMG losses included in the MPC cost (i)ideal absorbed power using Reactive control (ii)lossless power absorbed via MPC with N=160(16s) (iii)lossless power absorbed via MPC with N=40(4s) (iv)power absorbed with losses via MPC with N=160(16s) (v)power absorbed with losses via MPC with N=40(4s)

B. Electrical power maximisation

The electrical power optimisation cost function used is shown in (28). The results for this optimisation are shown in Fig. 6. From these results it is clearly shown that by including the losses in the cost function there has been a great improvement in the extraction of average electrical power, when compaired to Fig.5.

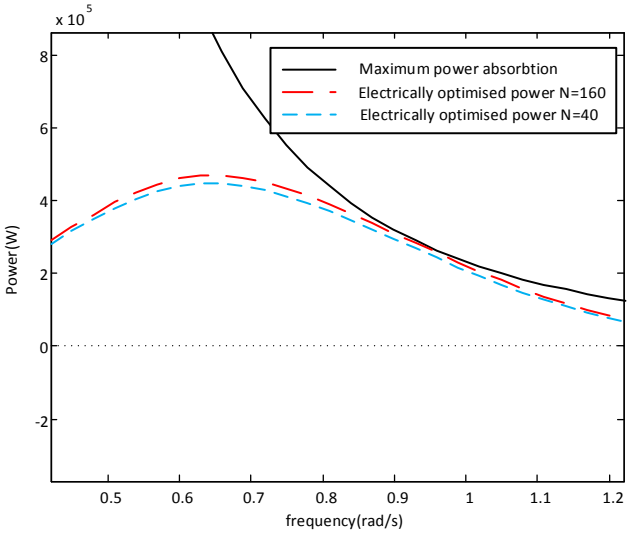

Fig. 6. Average power extracted from monochromatic waves with R=0.27Ω (i)ideal power via Reactive control (ii)electrical power optimisation MPC with N=160 (iii)electrical power optimisation MPC with N=40

C. Constraints

Introducing the resistance of the LPMG in the optimisation in the previous sub-section added more authenticity to the real life application. However when the LPMG has been examined closer [17] it becomes apparent that other restrictions may be necessary in the optimisation. Restrictions such as LPMG heave displacement, maximum current and converter voltage saturations and power rating. The main restrictions examined in this paper are the current saturation and the heave displacement saturation. Such constraints can easily be accommodated with Quadratic Programming in MATLAB, which works only with linear constraints. Other optimisation packages such as AMPL can accommodate non-linear constraints. The current and heave restrictions are linear constraints whilst other constraints such as converter voltage would be non-linear - MATLAB is therefore suitable for use in this paper.

The constraints for the current and heave displacement are shown below (30) and (31).

$$\frac{F_{min}}{\lambda'_{fd}\frac{\pi}{\tau}} \leq i_q(k) \leq \frac{F_{max}}{\lambda'_{fd}\frac{\pi}{\tau}} \tag{30}$$

$$z_{min} \leq z(k) \leq z_{max} \tag{31}$$

The hard constraints on the QP have to be in terms of the optimisation variable $\Delta u(k)$. The conversion of the currents and displacements into a function with only the optimisation variable is shown in (32) and (33). By combining (31) and the future values of $z(k)$ from (17) the hard constraints can be constructed (33).

$$(u_{min} - u_z(k-1))\,\mathbf{1} \leq \mathbf{\Phi}\boldsymbol{\Delta}\hat{\boldsymbol{u}}_{\boldsymbol{z}}(k) \leq (u_{max} - u_z(k-1))\,\mathbf{1} \tag{32}$$

$$\begin{aligned} WHa\boldsymbol{\Delta}\hat{\boldsymbol{u}}_{\boldsymbol{z}}(k) &\leq -WP\boldsymbol{x}_{\boldsymbol{z}}(k) - WHw\boldsymbol{\Delta}\hat{\boldsymbol{v}}_{\boldsymbol{z}}(k) + 1z_{max} \\ -WHa\boldsymbol{\Delta}\hat{\boldsymbol{u}}_{\boldsymbol{z}}(k) &\leq +WP\boldsymbol{x}_{\boldsymbol{z}}(k) + WHw\boldsymbol{\Delta}\hat{\boldsymbol{v}}_{\boldsymbol{z}}(k) + 1z_{min} \end{aligned} \tag{33}$$

where $K = \begin{bmatrix} 1 & 0 & 0 & 0 \end{bmatrix}$

$$\mathbf{\Phi} = \begin{bmatrix} 1 & 0 & 0 & \dots & 0 \\ 1 & 1 & 0 & \dots & 0 \\ & & & \ddots & \\ : & : & : & & : \\ 1 & 1 & 1 & \dots & 1 \end{bmatrix} \in \mathbb{R}^{N\times N} \tag{34}$$

$$W = \begin{bmatrix} K & \dots & \dots & \mathbf{0} \\ \dots & K & \dots & \mathbf{0} \\ & & \ddots & \\ : & : & & : \\ \dots & \dots & \dots & K \end{bmatrix} \in \mathbb{R}^{N\times 4N}$$

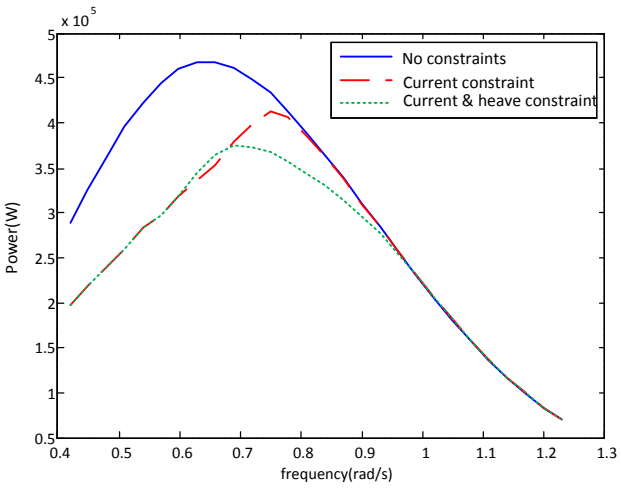

Fig. 7. Average power extracted from monochromatic waves via electrical power optimised MPC with N=100 and R=0.27Ω and (i) no constraints (ii) current constraint (iii) current and heave constraint

Fig. 7 shows the results of the MPC under various constraints with a receding horizon of 10 seconds ($N = 100, T_L = 0.1s$). From the data it can be concluded that as more constraints are introduced into the system the more the average real power is reduced at certain frequencies. The current constrained MPC shows that the power has significantly decreased overall but is still producing a positive average real power. The only section of the spectrum that the force restriction does not have much effect on is around the natural frequency. This occurs because the LPMG does not have to produce a great amount of force to force the velocity of the WEC into phase with the excitation force, at frequencies close to its natural frequency.

When a heave constraint is also introduced the average real power is reduced around the natural frequency as the heave displacements would not have been restricted as much with just a current constraint. Fig. 8 shows that when there were no constraints on the system the heave displacements and currents were impractical. When the constraints are introduced into the optimisation the heave and force of the PTO stay within their limits. It is shown in Fig. 9 that the non-linear PTO force is enforced to ensure the heave displacement stays within its limits.

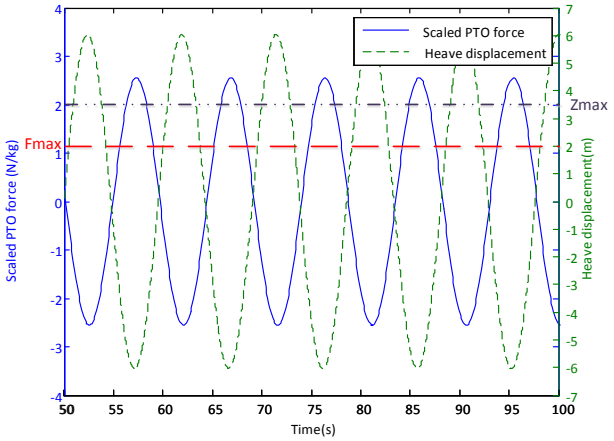

Fig. 8. Electrical power optimised MPC from monochromatic waves without constraints (i)scaled PTO force with saturation level (ii)heave displacement with saturation level

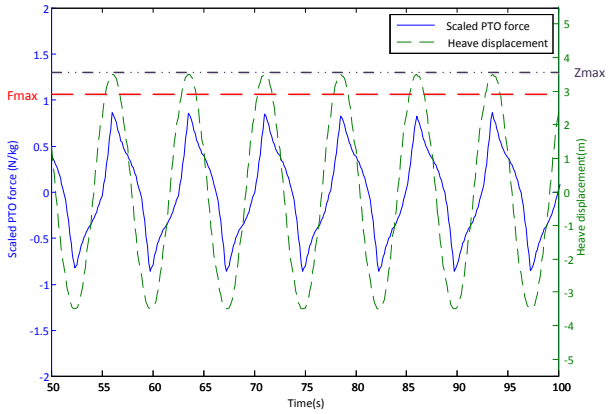

Fig. 9. Electrical power optimised MPC from monochromatic waves with heave and current constraints (i) scaled PTO force within its saturation level (ii)heave displacement within its saturation level

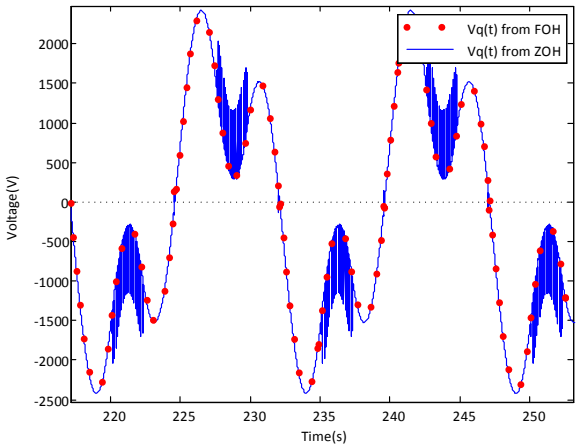

Fig. 10. q-axis voltage produced from the voltage source converter produced from monochromatic waves at $0.418\ rad/s$ (i)FOH MPC (ii)ZOH MPC

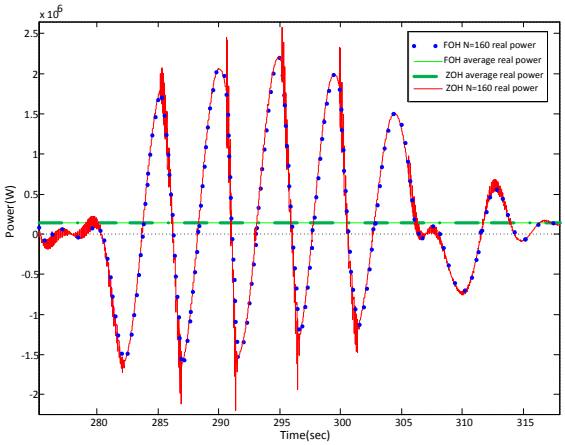

Fig. 11. Constrained current and heave displacement instantaneous electrical power with R=0.27Ω from a Bretscheinder spectrum using (i)FOH MPC N=160(16s) (ii)FOH average power (iii)ZOH average power (iv)ZOH MPC N=160(16s)

D. Power Quality

Up to this point in the paper all the results shown have been from an MPC system based on the ZOH method. The inner electrical controllers of the LPMG utilise a much faster sampling time than the outer mechanical loop of the system (Fig. 4)-this allows for the programming of the current setpoints with faster sampling to be piecewise linear over the long mechanical sampling time. As mentioned before the difference of the average power absorption between the ZOH and the FOH is inconsequential, since the ZOH method is an adequate estimation. However when the instantaneous power is examined between the ZOH and FOH constructed systems the difference is clear. With the ZOH the converter voltages are corrupted with high speed transients when the machine is moving with a high velocity. The converter voltages for the FOH based system look like a filtered version of the ZOH converter voltages, as can be seen in Fig. 10. Over an average time period this would not be a problem however this would lead to poor power quality, unnecessary high harmonics on the grid, unavoidable instantaneous overvoltages which could lead to permanent damage to the LPMG, the machine side converter and the grid side converter.

The simulated waveform shown in Fig. 11 displays the instantaneous powers from the ZOH and FOH systems extracted from a Bretschneider Spectrum with a significant height $H_s = 3m$ and a significant wave period $T_s = 0.9rad.s^{-1}$ [27]. The combination of the voltage spikes in the ZOH converter voltage and the overshoots in the current transients produce high frequency transients in the instantaneous power.

The current setpoints for the LPMG for a FOH system are effectively linearly interpolated over the outer sampling time, unlike the piecewise constant setpoints used by the ZOH outer loop as seen in Fig. 2. The sampling time of the LPMG ($T_{gen} = 1 \times 10^{-3}s$) is much smaller then the outer loop sampling time. This means that the inner control of the LPMG has a reference current which is changing linearly and gradually over the outer sample time. With the ZOH there is a sudden change in the reference current sent to the inner LPMG loop which is kept constant for the outer sampling time duration. These sharp steps in the current reference cause these overshoots. With the combination of the current waveforms and the voltages that do not contain spikes, the clean instantaneous power waveforms shows that a cascade

controller with a FOH in the outer slower loop is essential for better power quality.

The quality of the instantaneous power can be examined using a spectrum analyser (Fig. 12). With the spectrum analysis it is shown that the power from the FOH system at frequencies higher than the Bretschneider spectrum bandwidth are superior when compared to the powers from the ZOH system. This reduction of noise at higher frequencies could reduce the design complexity of components connected to the grid.

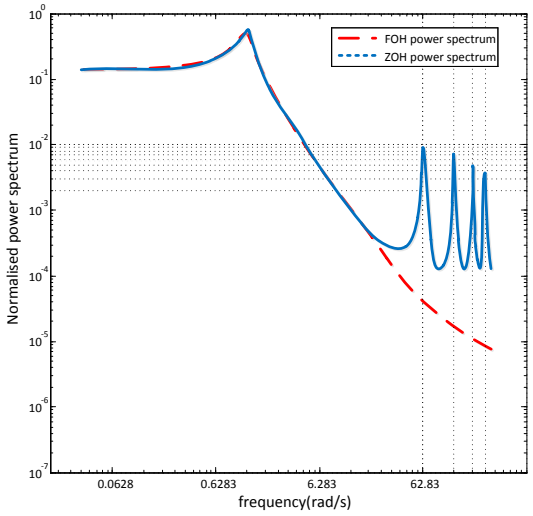

Fig. 12. Normalised power spectrum of the instantaneous electrical power from a (i)FOH MPC (ii)ZOH MPC which was excited by a Bretschneider spectrum

VI. Conclusion

This paper investigated the optimisation of average electrical power from the LPMG and a point absorber WEC connected via a fully rated back to back voltage source converter to the grid. The importance of the optimisation of electrical power was shown in section IV-A and V-A. When average mechanical power optimisation is employed the electrical power was unsatisfactory due to the electrical losses associated with the substantial PTO forces that were required.

In section IV-B and V-B the electrical power optimisation was implemented and results were shown. When current and heave displacement restrictions were introduced, the average electrical power moderately decreased when compared to the system with no constraints. The reduction in electrical power from the extracted mechanical power is dramatic for frequencies less than the WEC natural frequency.

The usual objective of wave energy has been to maximise the average mechanical PTO power. Whilst in this paper one of the objectives was to show the importance of optimising the electrical power from the LPMG, the other objective was to show the importance of the power quality which will be transmitted onto the grid. The results from section V-D showed that by using a FOH instead of a ZOH in the outer control loop, yields a significant increase in power quality.

Acknowledgment

This work was supported by the SFI Centre for Marine Renewable Energy Research (12/RC/2302).

References

[1] J. Budal, K. and Falnes, "Optimum operation of improved wave-power converter," *Marine Science Communications*, vol. 3, pp. 133–150, 1977.

[2] M. Folley and T. Whittaker, "The effect of sub-optimal control and the spectral wave climate on the performance of wave energy converter arrays," *Applied Ocean Research*, vol. 31, no. 4, pp. 260–266, Oct. 2009.

[3] F. Fusco and J. V. Ringwood, "Suboptimal Causal Reactive Control of Wave Energy Converters Using a Second Order System Model WEC," in *Proceedings of the 21st International Offshore and Polar Engineering Conference*, 2011, pp. 1–8.

[4] J. Falnes and K. Budal, "Wave - power conversion by point absorbers," *Norwegian Maritime research*, vol. 6, pp. 1–11, 1978.

[5] A. Babarit and A. H. Clément, "Optimal latching control of a wave energy device in regular and irregular waves," *Applied Ocean Research*, vol. 28, pp. 77–91, 2006.

[6] E. Abraham and E. C. Kerrigan, "Optimal active control and optimization of a wave energy converter," *IEEE Transactions on Sustainable Energy*, vol. 4, pp. 324–332, 2013.

[7] J. M. Maciejowski, *Predictive Control: With Constraints*, ser. Pearson Education. Prentice Hall, 2002.

[8] F. Fusco and J. V. Ringwood, "A simple and effective real-time controller for wave energy converters," *IEEE Transactions on Sustainable Energy*, vol. 4, pp. 21–30, 2013.

[9] ——, "Short-term wave forecasting for real-time control of wave energy converters," *IEEE Transactions on Sustainable Energy*, vol. 1, pp. 99–106, 2010.

[10] B. Quine, J. Uhlmann, and H. Durrant-Whyte, "Implicit Jacobian for linearised state estimation in nonlinear systems," *Proceedings of 1995 American Control Conference - ACC'95*, vol. 3, 1995.

[11] J. A. M. Cretel, A. W. Lewis, G. Lightbody, and G. P. Thomas, "An Application of Model Predictive Control to a Wave Energy Point Absorber," in *Proceedings of the IFAC Conference on Control Applications in Marine Systems*, 2010, pp. 1–6.

[12] J. A. M. Cretel, G. Lightbody, G. P. Thomas, and A. W. Lewis, "Maximisation of energy capture by a wave-energy point absorber using model predictive control," in *IFAC Proceedings Volumes (IFAC-PapersOnline)*, vol. 18, 2011, pp. 3714–3721.

[13] G. Li and M. R. Belmont, "Model predictive control of sea wave energy converters - Part I: A convex approach for the case of a single device," *Renewable Energy*, vol. 69, pp. 453–463, 2014.

[14] A. F. d. O. Falcão, "Phase control through load control of oscillating-body wave energy converters with hydraulic PTO system," *Ocean Engineering*, vol. 35, pp. 358–366, 2008.

[15] E. Tedeschi and M. Molinas, "Impact of control strategies on the rating of electric power take off for Wave Energy conversion," in *Proceedings of the IEEE International Symposium on Industrial Electronics*, 2010, pp. 2406–2411.

[16] R. Ekström, B. Ekergå rd, and M. Leijon, "Electrical damping of linear generators for wave energy convertersA review," *Renewable and Sustainable Energy Reviews*, vol. 42, pp. 116–128, 2015.

[17] H. Polinder, M. E. C. Damen, and F. Gardner, "Linear PM generator system for wave energy conversion in the AWS," *IEEE Transactions on Energy Conversion*, vol. 19, pp. 583–589, 2004.

[18] ——, "Design, modelling and test results of the AWS PM linear generator," in *European Transactions on Electrical Power*, vol. 15, 2005, pp. 245–256.

[19] N. Hodgins, O. Keysan, A. S. McDonald, and M. A. Mueller, "Design and testing of a linear generator for wave-energy applications," in *IEEE Transactions on Industrial Electronics*, vol. 59, 2012, pp. 2094–2103.

[20] F. Wu, X. P. Zhang, P. Ju, and M. J. H. Sterling, "Optimal Control for AWS-Based Wave Energy Conversion System," *Power Systems, IEEE Transactions on*, vol. 24, pp. 1747–1755, 2009.

[21] D. E. Montoya Andrade, A. De La Villa Jaén, and A. García Santana, "Considering linear generator copper losses on model predictive control for a point absorber wave energy converter," *Energy Conversion and Management*, vol. 78, pp. 173–183, 2014.

[22] W. E. Cummins, "The Impulse Response Function and Ship Motions," *Schiffstechnik*, vol. 9, pp. 101–109, 1962.

[23] WAMIT, *User manual*, 2006. [Online]. Available: http://wamit.com
[24] MATLAB, *version 7.10.0 (R2010a)*. Natick, Massachusetts: The MathWorks Inc., 2010.
[25] R. Fourer, D. M. Gay, M. Hill, B. W. Kernighan, and T. B. Laboratories, "AMPL : A Mathematical Programming Language," *Management Science*, vol. 36, pp. 519–554, 1990.
[26] N. Mohan, *Advanced Electric Drives: Analysis, Control, and Modeling Using MATLAB/Simulink*, 2014.
[27] C. L. Bretschneider, *Wave Variability and Wave Spectra for Wind-generated Gravity Waves*, ser. Technical memorandum. The Board, 1959.